Research Paper

Insulin-like growth factor-1 enhances neuroprotective effects of neural stem cell exosomes after spinal cord injury via an miR-219a-2-3p/YY1 mechanism

Ke Ma[1,*], Huiyou Xu[1,*], Jian Zhang[1,*], Fei Zhao[1], Haiqian Liang[1], Hongtao Sun[1], Ping Li[1], Sai Zhang[1], Renjie Wang[1], Xuyi Chen[1]

[1]Department of Neurosurgery, Characteristic Medical Center of Chinese People's Armed Police Force, Institution of Brain Trauma and Neurology Disease of People's Armed Police Forces, Tianjin Key Laboratory of Neurotrauma Repair, Tianjin 300162, China
*Equal contribution

Correspondence to: Renjie Wang, Xuyi Chen; **email:** renjie19870727@outlook.com, chenxuyi1979@sina.com.cn
Keywords: spinal cord injury (SCI), microRNAs (miRNAs), exosomes, apoptosis
Received: September 7, 2019 **Accepted:** November 23, 2019 **Published:** December 17, 2019

ABSTRACT

Spinal cord injury (SCI) remains the most common cause of paralysis, and there are no effective therapies for SCI patients. Neural stem cell (NSC)-derived exosomes can attenuate apoptosis and neuroinflammation after traumatic spinal cord injury, but the mechanisms underlying these effects remain unclear. Here, we examined the efficacy of miRNAs isolated from exosomes as treatments for SCI and characterized their mechanisms of action. Furthermore, we evaluated the effects of exosomes formed in the presence of insulin growth factor-1 (IFG-1, IGF-Exo), which promotes neural proliferation and regeneration, as well as normal exosomes (Nor-Exo) and compared control and H_2O_2-treated groups both *in vitro* and *in vivo*. Using microRNA sequencing and qRT-PCR, we identified miR-219a-2-3p, levels of which were higher in the IGF-Exo than Nor-Exo group and played crucial anti-inflammatory and anti-apoptosis roles. Additional experiments revealed that IGF-Exo inhibits YY1 expression through up-regulation of miR-219a-2-3p. This in turn inhibits the NF-κB pathway, partly inhibiting neuroinflammation and promoting the neuroprotective effects after SCI.

INTRODUCTION

Spinal cord injury (SCI), which typically results from traffic accidents or long falls, is the most common cause of paralysis [1]. Two key mechanisms play roles in the pathology of SCI: a) primary injury resulting from bruising and compressive lesions, and b) secondary injuries, including inflammation, formation of glial scars, microvascular bleeding, and upregulation of apoptotic factors, all of which inhibit axonal regeneration [2, 3]. There are no effective therapies for patients with SCI, and novel treatments are urgently needed.

Exosomes are nanosized extracellular vesicles 30–100 nm diameter which are formed as a result of inward budding in multiple cell types [4]. They were first discovered in sheep reticulocytes in 1983 [5], and the term "exosome" was coined by Johnstone in 1987 [6]. Exosomes may serve as biomarkers in many diseases due to the important role they play in intercellular communication and transport of proteins, mRNAs, and miRNAs into target cells [7, 8]. Exosomes can also have therapeutic effects in the nervous and respiratory systems [9]. Other studies demonstrated that exosomes derived from mesenchymal stem cells (MSCs) had therapeutic effects in liver, cardiovascular, and kidney diseases [10–12]. Furthermore, systemic administration of exosomes derived from MSCs promoted neurovascular reshaping and functional recovery after stroke in rats [13]. Exosomes can also reduce cognitive

impairments after traumatic brain injury [14]. Recent research has demonstrated that exosomes containing large amounts of miRNA are pivotal for intercellular communication in the nervous system [15]. The miRNAs contained in MSC-derived exosomes also play important roles in intercellular signaling more generally [16]. Current knowledge indicates that the process by which miRNAs are loaded into exosomes is not random and differs in different cell types [17]. In addition, a recent study suggests that exosomes facilitate the transfer of miR-155 from smooth muscle cells to endothelial cells, which induces endothelial injury and promotes atherosclerosis [18].

Although neural stem cell-derived exosomes attenuate apoptosis and neuroinflammation after traumatic spinal cord injury [19], the mechanism underlying this effect remains unknown. Because insulin-like growth factor-1 (IGF-1) promotes regeneration after neural injury and proliferation in neural cells [20–22], we hypothesized that it may enhance the protective and regenerative effects of NSC-derived exosomes after SCI.

The pathological effects of SCI are primarily a result of neuroinflammation, apoptosis, and oxidative stress injury [23–25]. We therefore established an H_2O_2-induced PC12 cell injury model to mimic SCI *in vitro* [26] and a rat SCI model using Allen's modified appliance *in vivo* [27, 28]. In this study, we examined the effects of IGF-1-induced (IGF-Exo) and normal exosomes (Nor-Exo) on neural inflammation, apoptosis, and regeneration after SCI and identified an miRNA-dependent mechanism responsible for those effects.

RESULTS

Preparation and characterization of IGF-Exo

Neural stem cells were obtained from E15 fetal rat cerebral cortex and cultured in medium until neurospheres of similar sizes and shapes formed (Fig. 1A). These neurospheres were immunopositive for the NSC marker nestin (shown in red) (Figure 1B). Rat NSCs collected from passage 3 were cultured in two kinds of culture medium: complete medium (DMEM/F12 medium supplemented with 20 ng/mL EGF, 10 ng/mL bFGF, 1× B27 supplement, 100 U/mL streptomycin, and 100 U/mL penicillin) or IGF-1 medium (100 ng/μL IGF-1 in complete medium). Exosomes were isolated from cell supernatants by ultracentrifugation. The shapes and sizes of both types of NSC-derived Exo were examined using transmission electron microscopy. While both the normal (Nor-Exo) and IGF-Exo had diameters of 30–300 nm, and the mean diameter of the IGF-Exo was slightly larger than

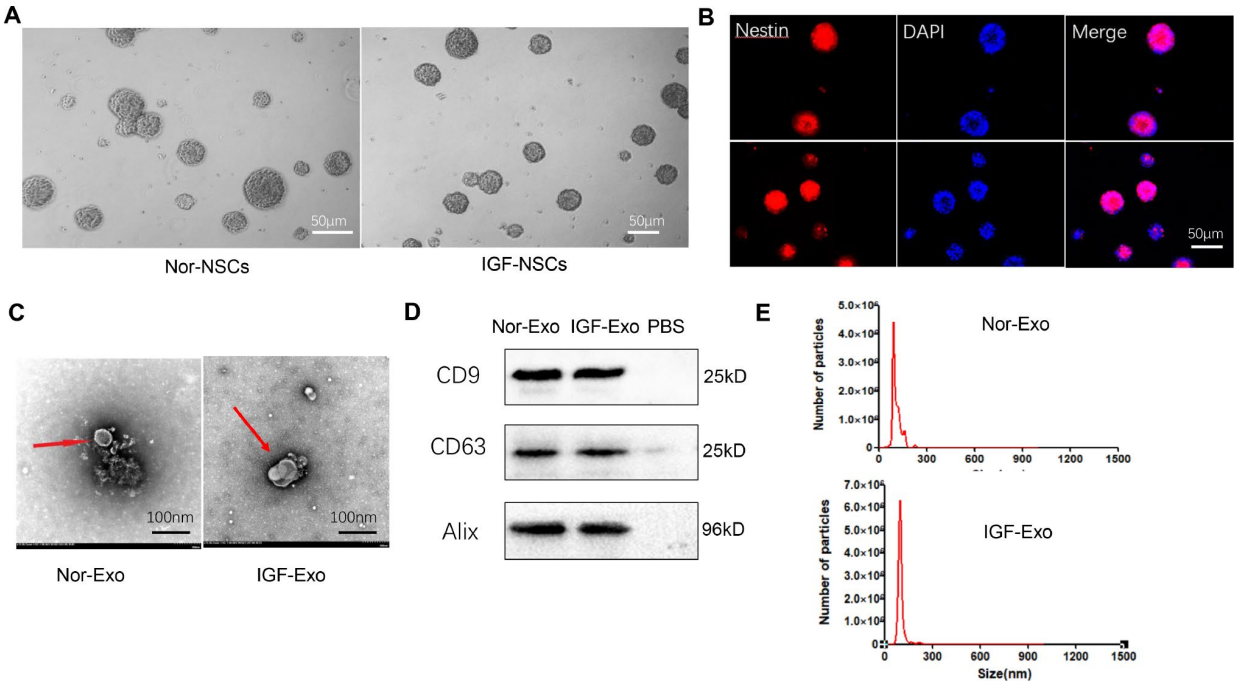

Figure 1. Characteristics of neural stem cells (NSCs) and exosomes derived from NSCs. (**A**) Morphology of neurospheres with typical shape examined by light microscopy. (**B**) Nestin immunofluorescence (red), a marker of NSCs, in neurospheres. (**C**) Exosome morphology examined by transmission electron microscopy. (**D**) Western blot analysis of exosome surface markers. (**E**) Particle size distribution of Nor-Exo and IGF-Exo by Nano Sight.

that of the Nor-Exo (Figure 1C). Western blot analysis indicated that levels of the exosomal markers CD9, CD63, and Alix were high in both Nor-Exo and IGF-Exo (Figure 1D). Nanosight analysis of Exo size distributions revealed that the mean diameters of Nor-Exo and IGF-Exo were 101.1 ± 19.0 nm and 139.3 ± 34.0 nm, respectively (Figure 1E).

IGF-Exo inhibits apoptosis and promotes regeneration in neural cells

We investigated the protective effect of IGF-Exo in PC12 cells treated with H_2O_2 to establish a cellular model of neural injury. CCK-8 assays showed that the 50% lethal dose of H_2O_2 was 200 μM for 24h in PC12 cells (Supplementary Figure 1A), and the optimal dose for IGF-1 in NSC culture was 200 ng/mL for 24h (Supplementary Figure 1B). After 24h of treatment with 200 μM H_2O_2, PC12 cells had damaged axons and decreased in number compared with the sham group. Additionally, cell viability was higher and axons were longer in IGF-Exo group PC12 cells than in the injury model group or Nor-Exo group ($P < 0.05$) (Figure 2A, 2B). In the TUNEL immunofluorescence assay, the ratio of TUNEL-positive cells in the IGF-Exo group was much higher than in the injury model group and slightly higher than in the Nor-Exo group ($P < 0.05$) (Figure 2C, 2D). To further explore the relationship between IFG-Exo and neural cell apoptosis, we measured Bax, Bcl-2, Beclin-1, and caspase-3 levels in

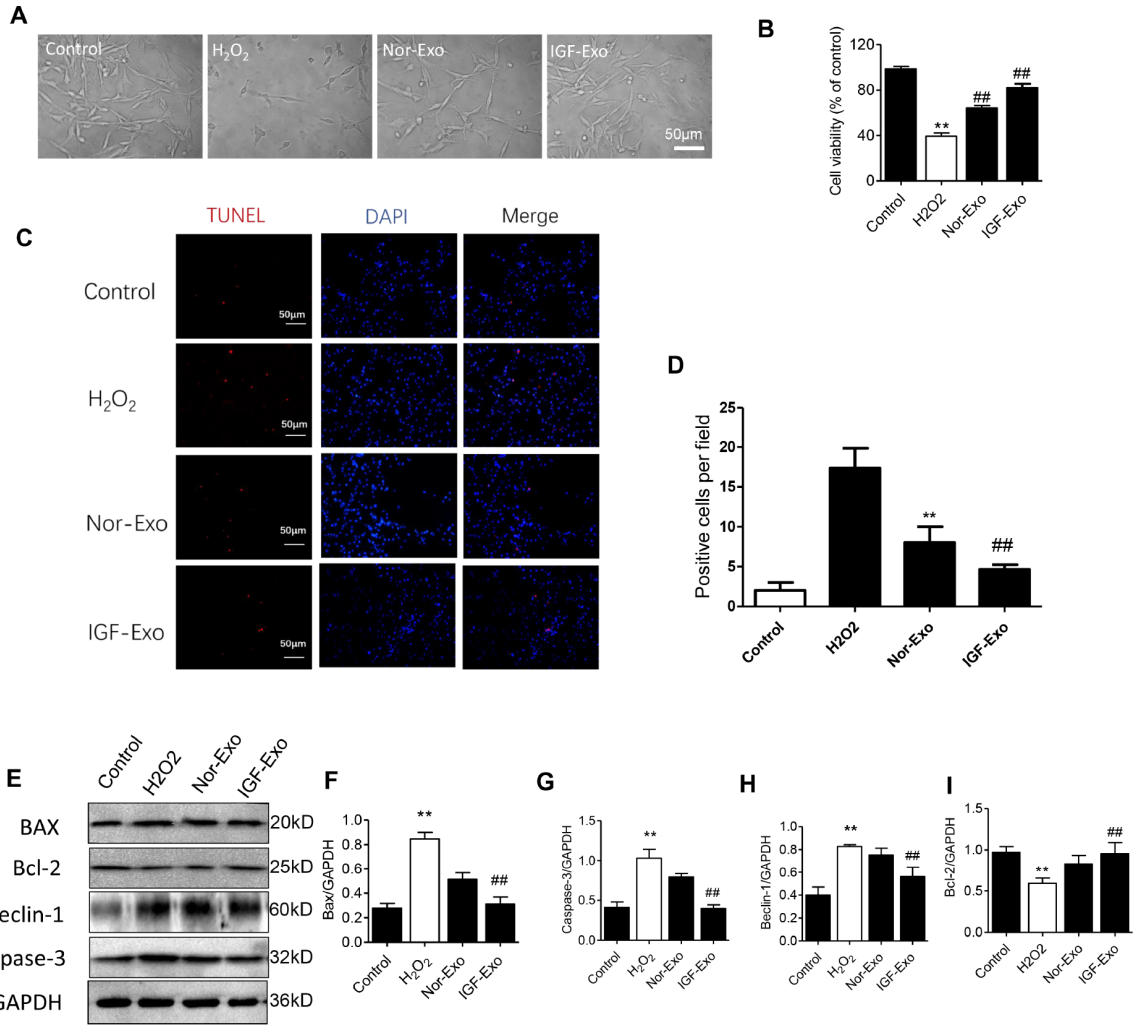

Figure 2. IGF-Exo inhibited H_2O_2-induced neural apoptosis in PC12 cells *in vitro*. (**A**) Morphology for each experimental group examined by light microscopy (control group: PC12 cells without treatment; H_2O_2 group: PC12 cells treated with H_2O_2 for 24h; Nor-Exo group: PC12 cells pretreated with Nor-Exo for 24h followed by H_2O_2 for 24h; IGF-Exo group: PC12 cells pretreated with IGF-Exo for 24h followed by H_2O_2 for 24h). (**B**) Cell viability in each experimental group; (**C**) TUNEL staining (red) indicating cell apoptosis in each experimental group; nuclear DAPI stain in blue. (**D**) TUNEL-positive cell numbers per field for each experimental group. (**E**) Western Blot analysis of apoptotic and anti-apoptotic proteins. (**F–I**) Relative expression of BAX, Bcl-2, Beclin-1 and Caspase-3. Data are expressed as means ± SD (analysis of variance followed by Student-Newman-Keuls *post hoc* test). ***P* < 0.01 *vs*. control group; ##*P* < 0.01 *vs*. H_2O_2 group.

the four PC12 cell groups. Compared with the sham group, Bax, Beclin-1, and caspase-3 expression were increased, while Bcl-2 expression decreased, in the injury group significantly increased ($P < 0.05$). Bax, Beclin-1, and caspase-3 expression were also higher in the IGF-Exo group than in the injury group or the Nor-Exo ($P < 0.05$) (Figure 2E–2I).

IGF-Exo reduces lesion size and promotes functional recovery after SCI

To test the neuroprotective effect of IGF-Exo *in vivo*, we established a rat model of acute SCI using a modified Allen's weight drop apparatus (Supplementary Figure 2). Rats received systemic IGF-Exo, sham, PBS, or Nor-Exo injections via the tail vein (Figure 3A). BBB locomotor scores were markedly lower in SCI group rats than in sham rats at 1, 3, 7, 14, and 28 days after SCI ($P < 0.01$). Compared with the SCI group, BBB scores were higher in Nor-Exo and IGF-Exo rats at 7, 14, and 28 days after SCI ($P < 0.05$). Moreover, the scores of IGF-Exo rats were higher than those of Nor-Exo rats at 14 and 28 days post-SCI ($P < 0.05$) (Supplementary Figure 3). MRI and neuroelectrophysiological examinations were also used to evaluate whether IGF-Exo promoted recovery from SCI recovery. DTI indicated that reconnection of the neural fasciculus was increased in the IGF-Exo group compared to the Nor-Exo and SCI groups (Figure 3B, Supplementary Figures 4, 5). Neuroelectrophysiological examination revealed that MEP amplitudes were higher in the IGF-Exo group than in the Nor-Exo and SCI groups (Figure 3C, 3D). In longitudinal sections of rat spinal cords collected for HE staining 28 days after SCI, injury areas (cavity) were smaller in the IGF-Exo group than in the SCI and Nor-Exo groups ($P < 0.05$) (Figure 3E, 3F). Immunostaining analysis of BrdU, a marker of new neurons, and NeuN, a general neural marker, revealed that BrdU and NeuN staining intensity were both lower in IGF-Exo group lesion areas than in the SCI and Nor-Exo groups at 28 days after SCI ($P < 0.05$) (Figure 3G). In a TUNEL assay performed 3 days after SCI, the TUNEL-positive cell (red) ratio was higher in the IGF-Exo group than in the injury model group and slightly higher than in the Nor-Exo group ($P < 0.05$) (Figure 3H, 3J).

Western blot analysis of Bax, Bcl-2, Beclin-1, and caspase-3 levels in the four groups of SCI rats were used to assess the anti-apoptosis effects of IGF-Exo *in vivo*. Compared with the sham group, Bax, Beclin-1, and caspase-3 expression increased, while Bcl-2 expression decreased, in the SCI group ($P < 0.05$). However, Bax, Beclin-1, and caspase-3 expression was significantly higher in the IGF-Exo group than in the SCI and Nor-Exo groups ($P < 0.05$) (Figure 3K–3O).

Antiapoptotic miR-219a-2-3p is highly increased in IGF-Exo

To illuminate the mechanism underling the neuroprotective effects of IGF-Exo, we characterized exosomal miRNA content though miRNA sequencing analysis. Six miRNAs were upregulated and 2 were downregulated in IGF-Exo compared to Nor-Exo (Figure 4A–4C; Supplementary Figure 6). qRT-PCR analysis was then performed to confirm that expression was higher for the 6 upregulated miRNAs identified in the sequencing analysis. All 6 miRNAs, namely rno-miR-138-5p ($P < 0.05$), rno-miR-219a-2-3p ($P < 0.05$), rno-miR-92b-3p ($P < 0.01$), rno-miR-92b ($P < 0.05$), rno-miR-25-5p ($P < 0.05$), and rno-miR-674-3p ($P < 0.01$), were significantly upregulated in IGF-Exo compared with Nor-Exo (Figure 4D).

Neuroprotective effects of IGF-Exo after SCI are associated with miR-219a-2-3p-dependent inhibition of YY1

We screened possible target genes of miR-219a-2-3p using bioinformatics methods (Target Scan v7.2) and identified YY1 was the potential target (Figure 5A). We therefore constructed a YY1-3′UTR (3′-Untranslated Region) expression vector containing a luciferase gene and transfected it into PC12 cells. A conventional luciferase reporter assay showed that miR-219a-2-3p interacted with YY1 (Figure 5A). Additionally, qRT-PCR showed that YY1 expression decreased when miR-219a-2-3p was upregulated (Figure 5B). Furthermore, YY1 expression increased when miR-219a-2-3p was downregulated (Figure 5C). Blockage of miR-219a-2-3p by Anti-miR-219a-2-3p (the miR-219a-2-3p inhibitor) inhibited IGF-Exo-mediated neuroprotective effects (Figure 5D). CCK-8 assays, TUNEL staining, and Western blots were performed to confirm that miR-219a-2-3p protected against neural injury and inhibited resulting apoptosis (Figure 5E–5G). The results indicated that miR-219a-2-3p expression down-regulated, while miR-219a-2-3p knockdown up-regulated, the YY1/NF-kB-p65 axis in PC12 cells (Figure 5H–5J).

DISCUSSION

Although basic research and clinical studies have attempted to identify more effective treatments for SCI patients, the prognosis remains very poor [29]. The pathological processes involved in SCI include neuroinflammation, apoptosis, and inhibition of neural regeneration [30, 31]. A previous study revealed that exosomes derived from MSC and NSC stem cells suppress inflammation and apoptosis after neural injury. However, the mechanisms underlying these effects

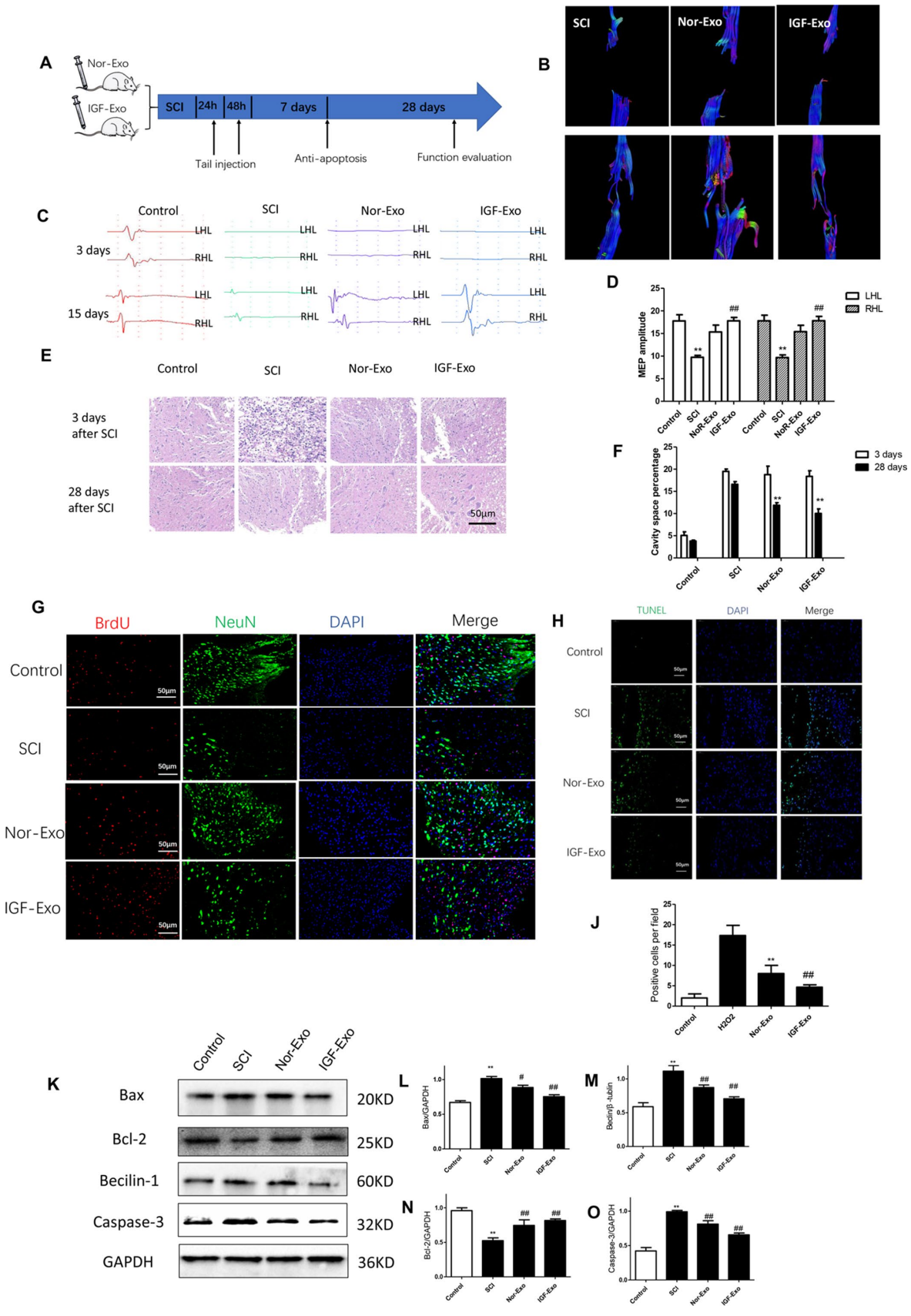

Figure 3. IGF-Exo inhibited neural apoptosis and neuroinflammation after SCI *in vivo*. (**A**) Schematic of tail intravenous injections of Nor-Exo and IGF-Exo in SCI model rats. (**B**) DTIs constructed for the SCI, Nor-Exo, and IGF-Exo groups at 1 day and 28 days after surgery. (**C**)

Neuroelectrophysiological examination results for each experimental group (control, SCI, Nor-Exo, and IGF-Exo) at 3 days and 28 days after surgery. (**D**) MEP amplitudes for each experimental group at 3 days and 28 days after surgery. (**E**) Hematoxylin-Eosin staining of sections containing SCI lesions in each experimental group at 3 days and 28 days after surgery. (**F**) Cavity space percentages for each experiment group at 3 days and 28 days after surgery. (**G**) BrdU and NeuN immunofluorescence indicative of neuron regeneration in each experimental group at 28 days after surgery. (**H**) TUNEL staining (green) indicative of apoptosis after SCI in each experimental group; DAPI in blue. (**J**) Numbers of TUNEL-positive cells per field for each experimental group. (**K–O**) Western Blot analysis of pro- and anti-apoptotic proteins (BAX, Bcl-2, Beclin-1, and Caspase-3). Data are expressed as means ± SD (analysis of variance followed by Student-Newman-Keuls *post hoc* test). **P < 0.01, *vs*. control group; ##P < 0.01, *vs*. SCI group.

remain unknown. Here, we used exosomes derived from NSCs exposed to IGF-1 to treat SCI for the first time and demonstrated that these IGF-Exo enhanced the neuroprotective effects of exosomes by inhibiting apoptosis and neuroinflammation in an miR-219a-2-3p-dependent manner.

Several studies have demonstrated that stem cells (especially MSCs and NSCs) administered either systemically or via local transplantation are potential therapies for neural injury and nervous system diseases [32]. However, stem cell therapies face important challenges. Tumorigenesis due to chromosome instability and distal vascular occlusion resulting from the large size of stem cells can be fatal, and the survival rate of stem cells *in vivo* is relatively low [33, 34]. Fortunately, increasing evidence suggests that the biological effects of stem cells can mostly be attributed to molecules they secrete, including those secreted via exosomes [9, 35]. Recent studies indicated that exosomes derived from NSCs might aid in the discovery of treatments for central nervous system

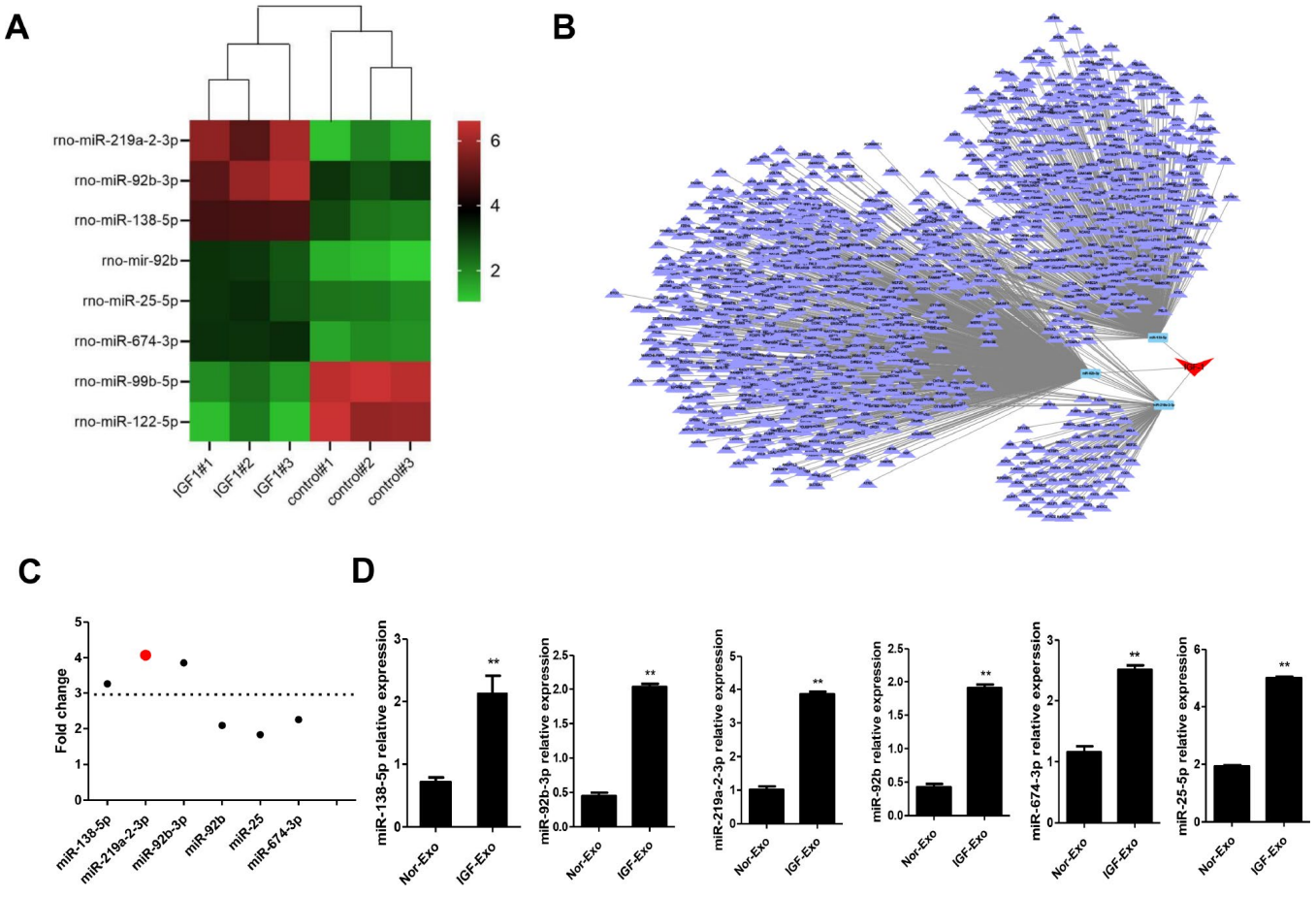

Figure 4. Screening and identification of upregulated miRNAs in Nor-Exo and IGF-Exo. (**A**) Heat map showing the 6 miRNAs for which expression was upregulated ≥ 2-fold in IGF-Exo compared to Nor-Exo. (**B**) IGF-1-induced miRNA regulation network. (**C**) Among the 6 upregulated miRNAs, miR-219a-2-3p expression increased the most. (**D**) qRT-PCR comparison of rno-miR-219a-2-3p, 138-5p, 92b-3p, 92b, 25-5p, and 674-3p expression between Nor-Exo and IGF-Exo from 3 independent experiments. *P < 0.05, **P < 0.01 for IGF-Exo *vs*. Nor-Exo.

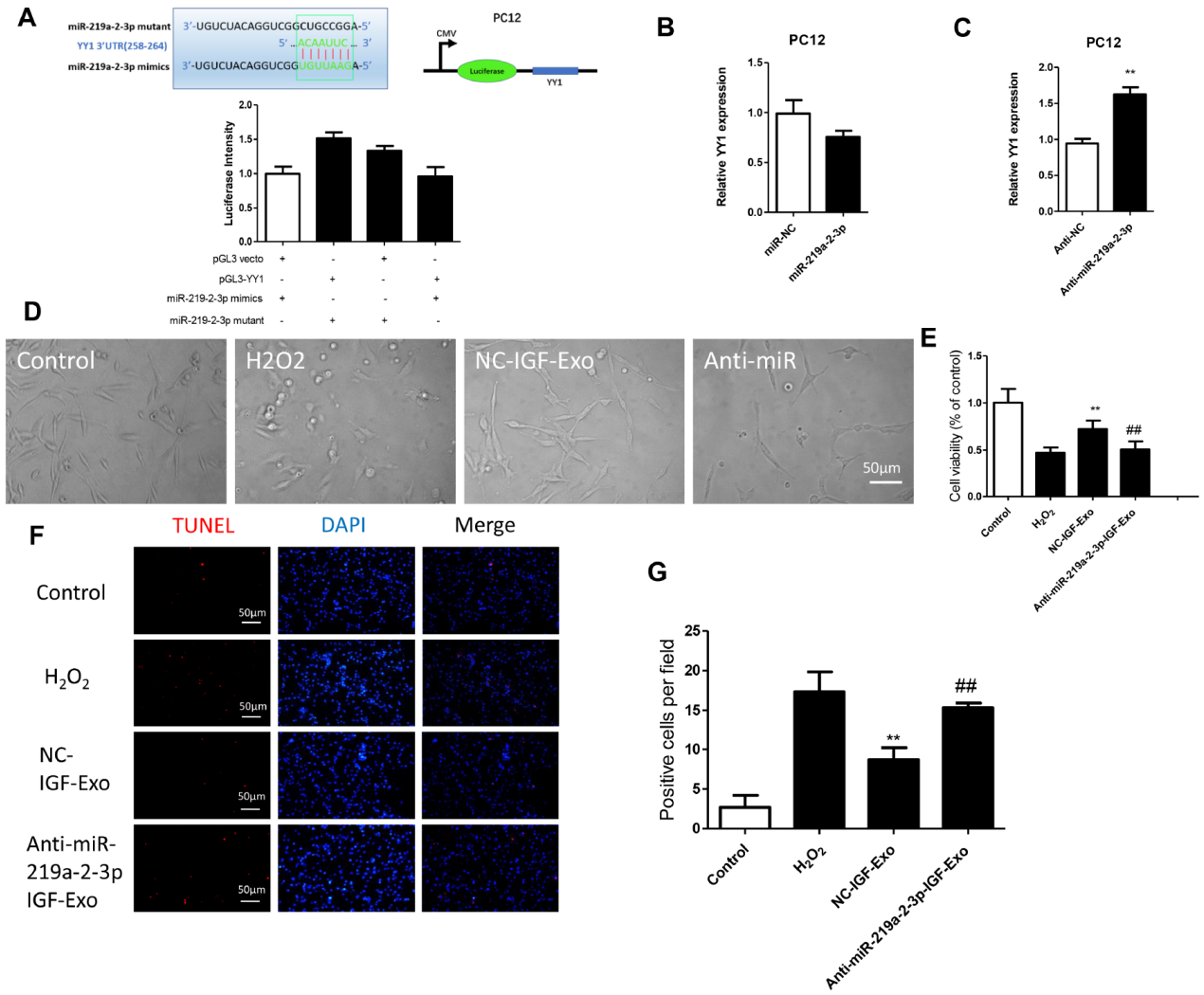

Figure 5. Inhibition of miR-219a-2-3p in exosomes reduced the protective effects of IGF-Exo. (**A**) Luciferase activity was detected in PC12 cells co-transfected with pGL3 vector, pGL3-YY1, miR-219a-2-3p mimics, or miR-219a-2-3p mutant. (**B**) Relative YY1 expression after upregulation of miR-219a-2-3p measured by qRT-PCR. B) PC12 cells were transfected with miR-219a-2-3p mimics or miR-NC; relative YY1 expression was analyzed by qRT-PCR. (**C**) PC12 cells were transfected with Anti-miR-219a-2-3p (miR-219a-2-3p inhibitor) or Anti-NC (control); relative YY1 expression was analyzed by qRT-PCR. (**D**) Morphology in each experimental group examined by light microscopy (control group: PC12 cells without treatment; H_2O_2 group: PC12 cells treated with H_2O_2 for 24h; IGF-Exo group: PC12 cells pretreated with IGF-Exo for 24h followed by H_2O_2 for 24h); Anti-miR-219a-2-3p-IGF-Exo group: PC12 cells pretreated with miR-219a-2-3p inhibitor-transfected IGF-Exo for 24h followed by H_2O_2 for 24h). (**E**) Cell viability in each experimental group when miR-219a-2-3p was downregulated in IGF-Exo; (**F**) TUNEL staining (red) indicative of apoptosis in each experimental group; DAPI in blue. (**G**) Numbers of TUNEL-positive cells per field for each experiment group. (**H–J**) Western Blot analysis of YY1 and NF-kB-p65 (si-NC: siRNA blank vector; miR-NC: miRNA blank vector; si-YY1: YY1 siRNA; miR-219a-2-3p: miR-219a-2-3p mimics). Data are expressed as means ± SD (analysis of variance followed by Student-Newman-Keuls *post hoc* test). ***P* < 0.01, *vs*. control group; ##*P* < 0.01, *vs*. SCI group.

injury [36, 37], but the mechanisms underlying their protective effects are unknown, and NSCs produce relatively small quantities of exosomes.

IGF-1 improves proliferation and metabolism in neural cells, and we confirmed this IGF-1-induced increase in NSC cell viability here in a CCK-8 assay. Exosomes play an important role in intercellular communication by transmitting bioactive RNAs and proteins, and exosomes derived from NSCs have therapeutic effects against ischemia and neurodegeneration [38, 39]. Because exosomes derived from NSCs can reduce apoptosis and neuroinflammation after SCI, we hypothesized that IGF-Exo could enhance these protective effects and promote regeneration after SCI.

In this study, RNA sequencing of Nor-Exo and IGF-Exo identified 8 microRNAs that were differentially expressed between the two exosome types, and miR-219a-2-3p was determined to the most significant among them. The difference in miR-219a-2-3p expression between Nor-Exo and IGF-Exo was verified by qRT-PCR assay. Previous research indicated that miR-219a-2-3p is enriched in human white matter and oligodendrocytes, and may be a potential target in demyelinating disorders [40]. Moreover, bioinformatics screening revealed that miR-219a-2-3p interacts with the downstream gene YY1 [41]. Here, a luciferase assay confirmed that up-regulation of miR-219a-2-3p inhibited YY1 expression, while changes in YY1 expression had no effect on the expression of miR-219a-2-3p. However, YY1 expression is correlated with activity of the inflammatory NK-kB pathway, and up-regulation of YY1 enhanced inflammatory effects. Therefore, IGF-Exo likely inhibits the expression of YY1, and in turn NK-kB pathway activity, through the up-regulation of miR-219a-2-3p, thus inhibiting neuroinflammation and promoting neuroprotective effects. This mechanism was confirmed in a rescue experiment in which miR-219a-2-3p expression was inhibited by transfection of si-miR-219a-2-3p.

Some important limitations of this study should be considered when interpreting the results and should be addressed in future studies. Firstly, additional *in vitro* studies are needed to fully characterize the mechanism underlying the neuroprotective effects of IGF-Exo, and their efficacy should be confirmed in clinical trials. Secondly, IGF-Exo might exert neuroprotective effects and inhibit the apoptosis and inflammation via the action of other miRNAs or pathways, and additional downstream genes of miR-219a-2-3p should be examined further. Finally, additional studies are needed to verify that the effects of miR-219a-2-3p on cell apoptosis and neural regeneration observed here are applicable in other *in vitro* cell models and under different conditions.

In summary, this study demonstrated that exosomes derived from neural stem cells exposed to IGF-1, at least partly, suppress the nerve inflammation, inhibit apoptosis, and promote nerve regeneration via an miR-219a-2-3p-dependent mechanism after the spinal cord injury. This is the first microRNA mechanism to be identified that might explain the effects of NSC-derived exosomes in SCI and may inform the development of novel treatments for spinal cord injury.

MATERIALS AND METHODS

Animals

Adult female Sprague-Dawley rats (180–200g) and pregnant rats (15d) were obtained from Beijing Vital River Laboratory Animal Technology Co., Ltd (Beijing, China). All animal care and experimental protocols were approved by the Ethics Committee of the Characteristic Medical Center of Chinese People's Armed Police Force. All animals were housed in individual cages on a 12h light/dark cycle with ad-libitum access to food and water.

Isolation and culture of rat embryonic NSCs

15-day embryos were isolated from pregnant rats euthanized with 230 mg/kg sodium pentobarbital. Cerebral cortex tissues were then isolated from the embryos and placed in Hank's solution. After the meninges were removed, the cerebral cortex was washed twice with Hank's solution, cut into pieces, digested with accutase cell detachment solution at 37°C for 10 min, and dispersed by pipetting. The suspension was filtered with a 200-mesh screen and then centrifuged at 800 rpm for 5 min; NSCs were obtained from the pelleted material. The cells were then re-suspended in complete medium (DMEM/F12 medium supplemented with 20 ng/ml EGF, 10 ng/ml bFGF, 1 × B27 supplement, 100 U/mL streptomycin, and 100 U/mL penicillin). After cell density was adjusted to 1×10^5/mL, cells were seeded into culture flasks and incubated at 37°C with 5% CO_2. After 3-5 days, cells were passaged. All NSCs used in this study were from passage 3.

Isolation and purification of NSC-Exo

Exosomes were isolated from NSC supernatant as previously described [42]. The medium was then collected and centrifuged at 300 × g for 10 min, followed by centrifugation at 2000 × g for 20 min at 4°C. After centrifugation, the supernatant was filtered using a 0.22 μm filter to remove dead cells and large

cellular debris. Small cellular debris were then pelleted by centrifugation at 10,000 × g for 30 minutes, and the supernatants were recentrifuged at 100,000 × g for 70 minutes. Finally, pelleted exosomes were resuspended in 100 μL PBS solution in the ultracentrifuge tubes. Exosomes were quantitated by measuring total protein concentration using a bicinchoninic acid assay (BCA; Thermo Fisher).

Identification of NSC-Exo

The morphology of NSC-derived exosomes (NSC-Exo) was assessed by transmission electron microscopy (TEM, Hitachi HT7700, Tokyo, Japan). Nanosizer™ technology (Malvern Instruments, Malvern, UK) was used to analyze the diameter distribution of NSC-Exo. Western blotting was used to examine the specific surface markers encapsulated in the exosomes, including CD9, CD63, and Alix.

***In vitro* experiment design**

In the first *in vitro* experiment, PC12 cells were divided among the following four groups to verify the protective effect of IGF-Exo: control group (untreated PC12 cells), H_2O_2 group (PC12 cells treated with H_2O_2 for 24h), Nor-Exo group (PC12 cells pretreated with Nor-Exo for 24h followed by H_2O_2 for 24h), and the IGF-Exo group (PC12 cells pretreated with IGF-Exo for 24h followed by H_2O_2 for 24h).

In the second *in vitro* experiment, PC12 cells were divided among the following four groups to verify the effects of miR-219a-2-3p: control group (untreated PC12 cells), H_2O_2 group (PC12 cells treated with H_2O_2 for 24h), NC-IGF-Exo group (PC12 cells pretreated with NC-IGF-Exo derived from IGF-1-induced NSCs transfected with miR inhibitor negative control (Anti-NC) for 24h followed by H_2O_2 for 24h), and Anti-miR-219a-2-3p-IGF-Exo group (PC12 cells pretreated with IGF-Exo derived from IGF-1-induced NSCs transfected with miR-219a-2-3p inhibitor (Anti- miR-219a-2-3p) for 24h followed by H_2O_2 for 24h).

***In vivo* experiment design**

Adult female Sprague-Dawley rats were divided among the following four groups (n=8 per group): control group (spinal cord segment T10 was only exposed in a sham operation), SCI group (acute SCI via modified Allen's weight drop apparatus, 0.5 mL PBS systemic administration through tail vein injection after SCI), Nor-Exo group (100 μg of precipitated normal exosome protein in 0.5 mL of PBS was administered via tail vein injection after SCI), and IGF-Exo group (100 μg of precipitated IGF-1-induced exosome protein in 0.5 mL of PBS was administered via tail vein injection after SCI).

Cell viability assay

The viability of PC12 cells and primary neurons was evaluated with a CCK-8 assay (Dojindo, Kumamoto, Japan) to examine the effects of NSC-Exo on neural cell proliferation. The cells were rinsed three times with 1 × PBS after 0, 24, 48, and 72 h of incubation. 10 μL of CCK-8 solution diluted in 90 μL of fresh culture medium was then added followed by incubated for another 2 h at 37°C.

Quantitative real-time RT-PCR

Total RNA was isolated from cells and tissues using Trizol reagent (TransGen Biotech, Beijing) according to the manufacturer's instructions. For RNase R treatment, 2 mg total RNA was incubated for 15 min at 37°C with or without 3 U/mg RNase R (Epicentre Technologies, Madison, WI, USA). qRT-PCR was performed using SYBR Green (TransGen Biotech) according to the manufacturer's instructions (Table 1) and an ABI 7500 real-time PCR instrument (Applied Biosystems, Foster City, CA, USA).

Transfection

Rat miR-219a-2-3p mimics, anti-miR-219a-2-3p (miR-219a-2-3p inhibitor), si-YY1 (si-YY1), miR mimics negative control (miR-NC), miR inhibitor negative control (miR-NC), and si-YY1 negative control (si-NC) were purchased from GenePharma (Shanghai, China). Sequences are listed in Table 2.

Cell apoptosis assays

PC12 cells were incubated with or without NSC-Exo (100 μg/mL) after treatment with H_2O_2 (200 μM) for 24 h. A terminal deoxynucleotidyl transferase-mediated dUTP nick end labeling assay (TUNEL; Roche, Basel, Switzerland) was used to detect DNA strand breaks according to the manufacturer's instructions. Images were captured using a fluorescence microscope (Leica, Solms, Germany). Apoptotic neuronal cells were determined by counting total numbers of TUNEL- and DAPI-stained cells.

Western blot analysis

Protein lysates were extracted from cells and 5 mm blocks of injured spinal cord tissue encompassing the lesion collected on days 3 and 28 after SCI by incubating with RIPA lysis and extraction buffer (KeyGEN Biotechnology, China). Protein concentration was

Table 1. Primers of miRNA used for qPCR in this study.

Primer	Sequence(5′to3′)
miR-138-5p	Forward: ACACTCCAGCTGGGAGCtGGtGttGTGAATC
	Reverse: TGGTGTCGTGGAGTCG
miR-219-2-3p	Forward: ACACTCCAGCTGGGAGAATTGTGGCTGGAC
	Reverse: TGGTGTCGTGGAGTCG
miR-25	Forward: ACACTCCAGCTGGGAGGCGGAGACACGGGC
	Reverse: TGGTGTCGTGGAGTCG
miR-674-3p	Forward: ACACTCCAGCTGGGCACAGCtCCCATCTCA
	Reverse: TGGTGTCGTGGAGTCG
miR-92b	Forward: ACACTCCAGCTGGGAGGGACGGGACGCGGTGC
	Reverse: TGGTGTCGTGGAGTCG
miR-92b-3p	Forward: ACACTCCAGCTGGGTATTGCACtCGTCCCG
	Reverse: TGGTGTCGTGGAGTCG
YY1	Forward: AGTGGGAACAGAAGCAGGTG
	Reverse: GAGGTCAATGCCAGGTATCC

Table 2. miRNA mimics, inhibitors, and siRNAs used in this study.

Name	Sequence(5′to3′)
miR-219a-2-3p mimics	AGAAUUGUGGCUGGACAUCUGU
miR-219a-2-3p inhibitor (Anti-miR-219a-2-3p)	ACAGAUGUCCAGCCACAAUUCU
siRNA-YY1(si-YY1)	GGUAAUAAGAAGUGGGAACTT
miR mimics negative control (miR-NC)	UUGUACUACACAAAAGUACUG
miR inhibitor negative control (Anti-NC)	CAGUACUUUUGUGUAGUACAA
si-YY1 negative control(si-NC)	UUCUCCGAACGUGUCACGUTT

determined using BCA. Equal amounts of proteins were separated by sodium dodecyl sulfate polyacrylamide gel electrophoresis, transferred to polyvinylidene difluoride membranes (EMD Millipore Corp., USA), incubated overnight at 4°C with primary antibodies, and blocked with bovine serum albumin (5%, v/v). The primary antibodies included Bax (1:2000, rabbit IgG; Abcam, USA), Bcl-2 (1:1000, rabbit IgG; Abcam, USA), Beclin-1 (1:1000, rabbit IgG; Abcam, USA), caspase-3 (1:1000, rabbit IgG; Abcam, USA), GAPDH (1:1000, Abcam, USA), YY1 (1:1000, mouse IgG1; Abcam, USA), and p65 (1:1000, rabbit IgG; Abcam, USA). The membranes were then incubated with secondary antibody (1:2000, Proteintech, USA) for 120 min at room temperature. Protein bands were visualized using enhanced chemi-luminescence reagent (Beyotime Institute of Biotechnology, Nanjing, China), and band density was analyzed semi-quantitatively using Image J software.

Immunofluorescence staining

For immunofluorescence staining, 1.0 x 10^5 NSCs were cultured in 0.5 mL media unless otherwise specified. Cultured cells were fixed with 4% (wt/vol) paraformaldehyde for 30 min at room temperature, washed with 0.1 M Tris-buffered solution (pH 7.5, TBS), blocked with 10% (vol/vol) normal goat serum in TBS containing 0.3% (vol/vol) Triton X-100 at room temperature for 60 min, and incubated with primary antibodies at 4°C overnight. The primary antibodies were rabbit anti-Nestin (1:1000), rabbit anti-BrdU (1:2000), and donkey anti-NeuN (1:1000). The cells were washed with TBS and incubated with Alexa Fluor 488- and 555-conjugated secondary antibodies (1:1000, Proteintech) at room temperature for 60 min. To visualize nuclei, the cells were counterstained with 2 μg/mL 4',6-diamidino-2-phenylindole (DAPI). Finally, the cells were mounted with 80% (vol/vol) glycerol, visualized under a fluorescent microscope (IX81, Olympus Corp., Tokyo, Japan), and image data were processed using MetaMorph (Molecular Devices, Sunnyvale, CA, USA) for quantification. Numbers of positive cells were counted in three to five fandom fields per well for three separate wells in each individual experiment.

Behavioral tests

Hindlimb motor function assessments were performed 1, 3, 7, 14, and 28 days after SCI using the Basso Beattie Bresnahan (BBB) locomotor rating scale and slanting board test. The BBB score ranged from 0 (complete

hindlimb paralysis) to 21 (normal locomotion). Scores were assigned by assessing the motor capacity of the experimental rats, including the movement of the hindlimbs, weight-bearing, and coordination of forelimb and hindlimb movements. The rats were placed in an open field of wooden models for 4 min and scored by 2 researchers using blinded methods. The slanting board test was performed according to the Rivlin method and involved placing a rat on a rectangular wooden oblique board covered with a rubber pad; the oblique plate was rotated to measure the angle of the inclined plate. When the longitudinal axis of the rat's body was parallel to the longitudinal axis of the inclined plate, the rat was tilted toward the side of the tilted plate to raise it in 5° increments. The maximum angle at which a rat could maintain its position for 5 s was measured. Measurements were performed five times for each animal, and the average values were analyzed.

Statistical analysis

The data are presented as means ± standard deviation (SD) and were analyzed using one-way analysis of variance and Tukey's *post hoc* multiple comparison tests. All experimental data were analyzed using SPSS 17.0. *P*-values < 0.05 were considered statistically significant. Additional experimental materials and methods details, including electrophysiological nerve and MRI assessments, are provided in the supplementary materials.

AUTHOR CONTRIBUTIONS

Ke Ma and Huiyou Xu performed statistical analysis and wrote the manuscript. Jian Zhang and Fei Zhao were involved in manuscript preparation. Renjie Wang and Xuyi Chen were responsible for study design and data collection. Haiqian Liang, Hongtao Sun, Ping Li, Sai Zhang, and Xuyi Chen were responsible for research funding. All authors approved the final version of the manuscript.

CONFLICTS OF INTEREST

None of the authors declare any conflicts of interest.

FUNDING

This study was support by the National Key Research and Development Plan of China (No. 2016YFC1101500), the National Natural Science Foundation of China (No. 11672332), the Key Science and Technology Support Foundation of Tianjin City (No. 17YFZCSY00620), the Major Project of Tianjin Science and Technology Military and Civilian Integration (No. 18ZXJMTG00260), and the Project of Tianjin Rescue Medicine Clinical Center (No. 15ZXLCSY00040).

REFERENCES

1. Huang JH, Yin XM, Xu Y, Xu CC, Lin X, Ye FB, Cao Y, Lin FY. Systemic Administration of exosomes released from mesenchymal stromal cells attenuates apoptosis, inflammation, and promotes angiogenesis after spinal cord injury in rats. J Neurotrauma. 2017; 34:3388–96. https://doi.org/10.1089/neu.2017.5063 PMID:28665182

2. Angeli C, Ochsner J, Harkema S. Effects of chronic baclofen use on active movement in an individual with a spinal cord injury. Spinal Cord. 2012; 50:925–27. https://doi.org/10.1038/sc.2012.93 PMID:22945743

3. Kong FL, Wang XP, Li YN, Wang HX. The role of exosomes derived from cerebrospinal fluid of spinal cord injury in neuron proliferation in vitro. Artif Cells Nanomed Biotechnol. 2018; 46:200–05. https://doi.org/10.1080/21691401.2017.1304408 PMID:28346015

4. Théry C, Zitvogel L, Amigorena S. Exosomes: composition, biogenesis and function. Nat Rev Immunol. 2002; 2:569–79. https://doi.org/10.1038/nri855 PMID:12154376

5. Harding C, Heuser J, Stahl P. Receptor-mediated endocytosis of transferrin and recycling of the transferrin receptor in rat reticulocytes. J Cell Biol. 1983; 97:329–39. https://doi.org/10.1083/jcb.97.2.329 PMID:6309857

6. Mathivanan S, Ji H, Simpson RJ. Exosomes: extracellular organelles important in intercellular communication. J Proteomics. 2010; 73:1907–20. https://doi.org/10.1016/j.jprot.2010.06.006 PMID:20601276

7. Pathan M, Keerthikumar S, Chisanga D, Alessandro R, Ang CS, Askenase P, Batagov AO, Benito-Martin A, Camussi G, Clayton A, Collino F, Di Vizio D, Falcon-Perez JM, et al. A novel community driven software for functional enrichment analysis of extracellular vesicles data. J Extracell Vesicles. 2017; 6:1321455. https://doi.org/10.1080/20013078.2017.1321455 PMID:28717418

8. Tkach M, Kowal J, Théry C. Why the need and how to approach the functional diversity of extracellular vesicles. Philos Trans R Soc Lond B Biol Sci. 2018; 373:20160479. https://doi.org/10.1098/rstb.2016.0479 PMID:29158309

9. Ratajczak MZ, Jadczyk T, Pędziwiatr D, Wojakowski W. New advances in stem cell research: practical implications for regenerative medicine. Pol Arch Med Wewn. 2014; 124:417–26. https://doi.org/10.20452/pamw.2355 PMID:24956404

10. Gatti S, Bruno S, Deregibus MC, Sordi A, Cantaluppi V, Tetta C, Camussi G. Microvesicles derived from human adult mesenchymal stem cells protect against ischaemia-reperfusion-induced acute and chronic kidney injury. Nephrol Dial Transplant. 2011; 26:1474–83. https://doi.org/10.1093/ndt/gfr015 PMID:21324974

11. Lai RC, Chen TS, Lim SK. Mesenchymal stem cell exosome: a novel stem cell-based therapy for cardiovascular disease. Regen Med. 2011; 6:481–92. https://doi.org/10.2217/rme.11.35 PMID:21749206

12. Li T, Yan Y, Wang B, Qian H, Zhang X, Shen L, Wang M, Zhou Y, Zhu W, Li W, Xu W. Exosomes derived from human umbilical cord mesenchymal stem cells alleviate liver fibrosis. Stem Cells Dev. 2013; 22:845–54. https://doi.org/10.1089/scd.2012.0395 PMID:23002959

13. Xin H, Li Y, Cui Y, Yang JJ, Zhang ZG, Chopp M. Systemic administration of exosomes released from mesenchymal stromal cells promote functional recovery and neurovascular plasticity after stroke in rats. J Cereb Blood Flow Metab. 2013; 33:1711–15. https://doi.org/10.1038/jcbfm.2013.152 PMID:23963371

14. Kim DK, Nishida H, An SY, Shetty AK, Bartosh TJ, Prockop DJ. Chromatographically isolated CD63+CD81+ extracellular vesicles from mesenchymal stromal cells rescue cognitive impairments after TBI. Proc Natl Acad Sci USA. 2016; 113:170–75. https://doi.org/10.1073/pnas.1522297113 PMID:26699510

15. Lotvall J, Valadi H. Cell to cell signalling via exosomes through esRNA. Cell Adh Migr. 2007; 1:156–58. https://doi.org/10.4161/cam.1.3.5114 PMID:19262134

16. Zhang B, Wu X, Zhang X, Sun Y, Yan Y, Shi H, Zhu Y, Wu L, Pan Z, Zhu W, Qian H, Xu W. Human umbilical cord mesenchymal stem cell exosomes enhance angiogenesis through the Wnt4/β-catenin pathway. Stem Cells Transl Med. 2015; 4:513–22. https://doi.org/10.5966/sctm.2014-0267 PMID:25824139

17. Hofer HR, Tuan RS. Secreted trophic factors of mesenchymal stem cells support neurovascular and musculoskeletal therapies. Stem Cell Res Ther. 2016; 7:131. https://doi.org/10.1186/s13287-016-0394-0 PMID:27612948

18. Zheng B, Yin WN, Suzuki T, Zhang XH, Zhang Y, Song LL, Jin LS, Zhan H, Zhang H, Li JS, Wen JK. Exosome-Mediated miR-155 Transfer from Smooth Muscle Cells to Endothelial Cells Induces Endothelial Injury and Promotes Atherosclerosis. Mol Ther. 2017; 25:1279–94. https://doi.org/10.1016/j.ymthe.2017.03.031 PMID:28408180

19. Rong Y, Liu W, Wang J, Fan J, Luo Y, Li L, Kong F, Chen J, Tang P, Cai W. Neural stem cell-derived small extracellular vesicles attenuate apoptosis and neuroinflammation after traumatic spinal cord injury by activating autophagy. Cell Death Dis. 2019; 10:340. https://doi.org/10.1038/s41419-019-1571-8 PMID:31000697

20. Hwang DH, Park HH, Shin HY, Cui Y, Kim BG. Insulin-like growth factor-1 receptor dictates beneficial effects of treadmill training by regulating survival and migration of neural stem cell grafts in the injured spinal cord. Exp Neurobiol. 2018; 27:489–507. https://doi.org/10.5607/en.2018.27.6.489 PMID:30636901

21. Sun P, Ortega G, Tan Y, Hua Q, Riederer PF, Deckert J, Schmitt-Böhrer AG. Streptozotocin impairs proliferation and differentiation of adult hippocampal neural stem cells in vitro-correlation with alterations in the expression of proteins associated with the insulin system. Front Aging Neurosci. 2018; 10:145. https://doi.org/10.3389/fnagi.2018.00145 PMID:29867451

22. Zhu H, Xue C, Yao M, Wang H, Zhang P, Qian T, Zhou S, Li S, Yu B, Wang Y, Gu X. miR-129 controls axonal regeneration via regulating insulin-like growth factor-1 in peripheral nerve injury. Cell Death Dis. 2018; 9:720. https://doi.org/10.1038/s41419-018-0760-1 PMID:29915198

23. Holmes D. Spinal-cord injury: spurring regrowth. Nature. 2017; 552:S49. https://doi.org/10.1038/d41586-017-07550-9 PMID:29239374

24. Zhang S, Fujita Y, Matsuzaki R, Yamashita T. Class I histone deacetylase (HDAC) inhibitor CI-994 promotes functional recovery following spinal cord injury. Cell Death Dis. 2018; 9:460. https://doi.org/10.1038/s41419-018-0543-8 PMID:29700327

25. Milich LM, Ryan CB, Lee JK. Correction to: the origin, fate, and contribution of macrophages to spinal cord injury pathology. Acta Neuropathol. 2019; 137:799–800. https://doi.org/10.1007/s00401-019-02016-w PMID:31011858

26. Luo Z, Wu F, Xue E, Huang L, Yan P, Pan X, Zhou Y. Hypoxia preconditioning promotes bone marrow mesenchymal stem cells survival by inducing HIF-1α in injured neuronal cells derived exosomes culture

system. Cell Death Dis. 2019; 10:134.
https://doi.org/10.1038/s41419-019-1410-y
PMID:30755595

27. Kjell J, Olson L. Rat models of spinal cord injury: from pathology to potential therapies. Dis Model Mech. 2016; 9:1125–37.
https://doi.org/10.1242/dmm.025833
PMID:27736748

28. Cao Y, Wu TD, Wu H, Lang Y, Li DZ, Ni SF, Lu HB, Hu JZ. Synchrotron radiation micro-CT as a novel tool to evaluate the effect of agomir-210 in a rat spinal cord injury model. Brain Res. 2017; 1655:55–65.
https://doi.org/10.1016/j.brainres.2016.11.015
PMID:27847197

29. Seo JY, Kim YH, Kim JW, Kim SI, Ha KY. Effects of therapeutic hypothermia on apoptosis and autophagy after spinal cord injury in rats. Spine. 2015; 40:883–90.
https://doi.org/10.1097/BRS.0000000000000845
PMID:25705963

30. Gensel JC, Zhang B. Macrophage activation and its role in repair and pathology after spinal cord injury. Brain Res. 2015; 1619:1–11.
https://doi.org/10.1016/j.brainres.2014.12.045
PMID:25578260

31. Gao L, Dai C, Feng Z, Zhang L, Zhang Z. MiR-137 inhibited inflammatory response and apoptosis after spinal cord injury via targeting of MK2. J Cell Biochem. 2018; 119:3280–92.
https://doi.org/10.1002/jcb.26489 PMID:29125882

32. Wu Q, Wang Q, Li Z, Li X, Zang J, Wang Z, Xu C, Gong Y, Cheng J, Li H, Shen G, Dong C. Human menstrual blood-derived stem cells promote functional recovery in a rat spinal cord hemisection model. Cell Death Dis. 2018; 9:882.
https://doi.org/10.1038/s41419-018-0847-8
PMID:30158539

33. Jeong JO, Han JW, Kim JM, Cho HJ, Park C, Lee N, Kim DW, Yoon YS. Malignant tumor formation after transplantation of short-term cultured bone marrow mesenchymal stem cells in experimental myocardial infarction and diabetic neuropathy. Circ Res. 2011; 108:1340–47.
https://doi.org/10.1161/CIRCRESAHA.110.239848
PMID:21493893

34. Wang X, Botchway BO, Zhang Y, Yuan J, Liu X. Combinational treatment of bioscaffolds and extracellular vesicles in spinal cord injury. Front Mol Neurosci. 2019; 12:81.
https://doi.org/10.3389/fnmol.2019.00081
PMID:31031590

35. Ratajczak MZ, Bujko K, Wojakowski W. Stem cells and clinical practice: new advances and challenges at the time of emerging problems with induced pluripotent stem cell therapies. Pol Arch Med Wewn. 2016; 126:879–90.
https://doi.org/10.20452/pamw.3644 PMID:27906881

36. Liu W, Wang Y, Gong F, Rong Y, Luo Y, Tang P, Zhou Z, Zhou Z, Xu T, Jiang T, Yang S, Yin G, Chen J, et al. Exosomes derived from bone mesenchymal stem cells repair traumatic spinal cord injury by suppressing the activation of A1 neurotoxic reactive astrocytes. J Neurotrauma. 2019; 36:469–84.
https://doi.org/10.1089/neu.2018.5835
PMID:29848167

37. Webb RL, Kaiser EE, Scoville SL, Thompson TA, Fatima S, Pandya C, Sriram K, Swetenburg RL, Vaibhav K, Arbab AS, Baban B, Dhandapani KM, Hess DC, et al. Human neural stem cell extracellular vesicles improve tissue and functional recovery in the murine thrombo-embolic stroke model. Transl Stroke Res. 2018; 9:530–39.
https://doi.org/10.1007/s12975-017-0599-2
PMID:29285679

38. Zhang Y, Kim MS, Jia B, Yan J, Zuniga-Hertz JP, Han C, Cai D. Hypothalamic stem cells control ageing speed partly through exosomal miRNAs. Nature. 2017; 548:52–57.
https://doi.org/10.1038/nature23282 PMID:28746310

39. Vogel A, Upadhya R, Shetty AK. Neural stem cell derived extracellular vesicles: attributes and prospects for treating neurodegenerative disorders. EBioMedicine. 2018; 38:273–82.
https://doi.org/10.1016/j.ebiom.2018.11.026
PMID:30472088

40. de Faria O Jr, Cui QL, Bin JM, Bull SJ, Kennedy TE, Bar-Or A, Antel JP, Colman DR, Dhaunchak AS. Regulation of miRNA 219 and miRNA Clusters 338 and 17-92 in Oligodendrocytes. Front Genet. 2012; 3:46.
https://doi.org/10.3389/fgene.2012.00046
PMID:22470405

41. Morozzi G, Beccafico S, Bianchi R, Riuzzi F, Bellezza I, Giambanco I, Arcuri C, Minelli A, Donato R. Oxidative stress-induced S100B accumulation converts myoblasts into brown adipocytes via an NF-κB/YY1/miR-133 axis and NF-κB/YY1/BMP-7 axis. Cell Death Differ. 2017; 24:2077–88.
https://doi.org/10.1038/cdd.2017.132
PMID:28885620

42. Théry C, Amigorena S, Raposo G, Clayton A. Isolation and characterization of exosomes from cell culture supernatants and biological fluids. Curr Protoc Cell Biol. 2006; Chapter 3:Unit 3.22.
https://doi.org/10.1002/0471143030.cb0322s30
PMID:18228490

SUPPLEMENTARY MATERIALS

Supplementary Methods

Cells and cell culture

PC12 cells were provided by the Riken Cell Bank (Tsukuba Science City, Japan), PC12 cells were maintained in RAPI 1640 medium, containing 10% FBS, 100 IU/mL penicillin, and 100 mg/mL streptomycin. All the medium was changed every 3 days, cells were passaged every 3–5 days, according to an established protocol, 32 primary neurons were collected from embryonic (E16–18) Sprague-Dawley (SD) rats. Briefly, cerebral cortices were isolated and dissociated with trypsin (0.25%, w/v; Thermo Fisher Scientific, USA) for 20 min. Neurons were seeded at a density of 5 × 104/mL for immunofluorescent staining in 24-well culture plates and 1 × 106/mL for western blot assays in 6-well culture plates. Neurons were maintained in fresh neurobasal medium (Thermo Fisher Scientific) containing 2% B27 (2%, w/v; Thermo Fisher Scientific), 1% glutamine (Thermo Fisher Scientific), 100 IU/mL penicillin, and 100 mg/mL streptomycin. Half of the medium was changed every third day. After 5 days of cell culture, the obtained neurons were examined by microtubule.

Luciferase reporter assay

Latent binding sites were predicted by the Target Scan database (http://www.targetscan.org). PC12 cells (1 × 105 cells/well) were added to a 24-well plate and co-transfected with 200 ng pGL3-LUC-YY1 or pGL3-LUC-control vector and 80 nmol miRNA mimics or miRNA mutant mimics. After 48 h of transfection, the cells were harvested, and luciferase activities were measured with the Dual-Luciferase Reporter Assay System (Promega, Madison, WI, USA).

SCI model

The rats were anesthetized and injected intraperitoneally with chloral hydrate (300 mg/kg). The incision area was sterilized with 75% alcohol, an incision was made, and the skin was separated, then a laminectomy was performed to expose spinal cord segment T10. The impactor (weighing 10 g, 3 mm in diameter, and 200 mm in length) was obtained from the Affiliated Hospital of the Logistics University of the Chinese People's Armed Police Force. The impactor was dropped from a height of 50 mm to the surface of the spinal cord. Successfully induced SCI resulted in spinal cord congestion, tail swing reflexes, swaying legs, and slow paralysis. The wound was sutured after the spinal cord was hit. All rats were kept in a separate environment at 24°C to ensure adequate water, food, and clean bedding. The rats were provided intermittently with assisted urination 3 times daily.

MRI

While the animals were under general anesthesia, MRI scans and DTI constructions were performed by using the Siemens MAGNETOM Verso 3.0T MRI system. Since vitamin E is a fat-soluble substance that elicits high signals during MRI scanning and DTI construction, we used a vitamin E capsule as a simple marker to assist DTI to locate the scope of injury .

Nerve electrophysiological assessment

Electrophysiological assessments were including preoperative, intraoperative and postoperative measurements of the MEP for the limbs using an evoked potential (EP) instrument Viking Quest (Thermo Nicolet Corporation, USA). For preoperative measurement, amplitude and latency of the MEP were assessed: amplitude was the peak-to-peak voltage, meaning the potential difference between the most positive and the most negative peaks, and latency was time between the start of the stimulus to the appearance of the initial response wave.

Supplementary Figures

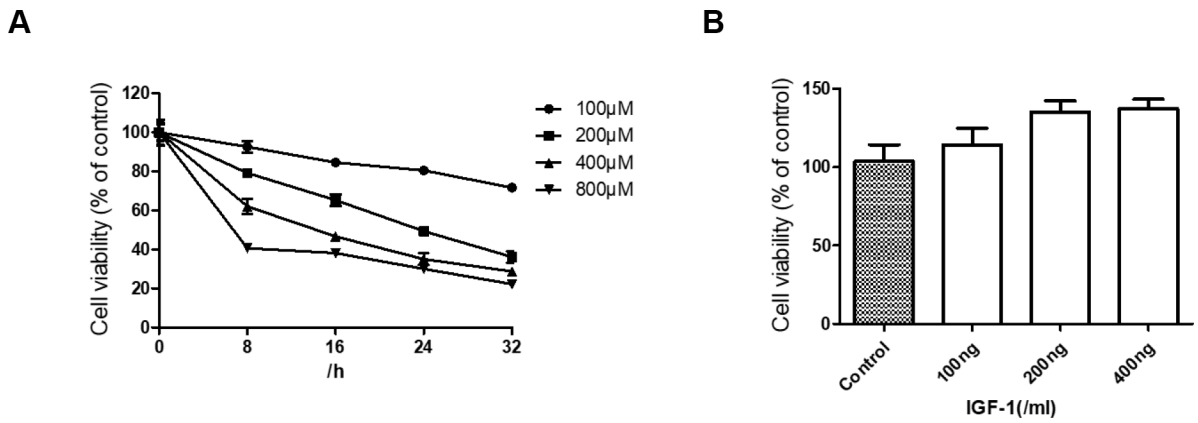

Supplementary Figure 1. IGF-Exo reduces apoptosis and promotes regeneration in neurons *in vitro*. (**A**) The CCK-8 assay of cell viability of different dose and different time of H_2O_2 on PC12 cells; (**B**) The viability of NSCs that different concentration of IGF-1 treatment.

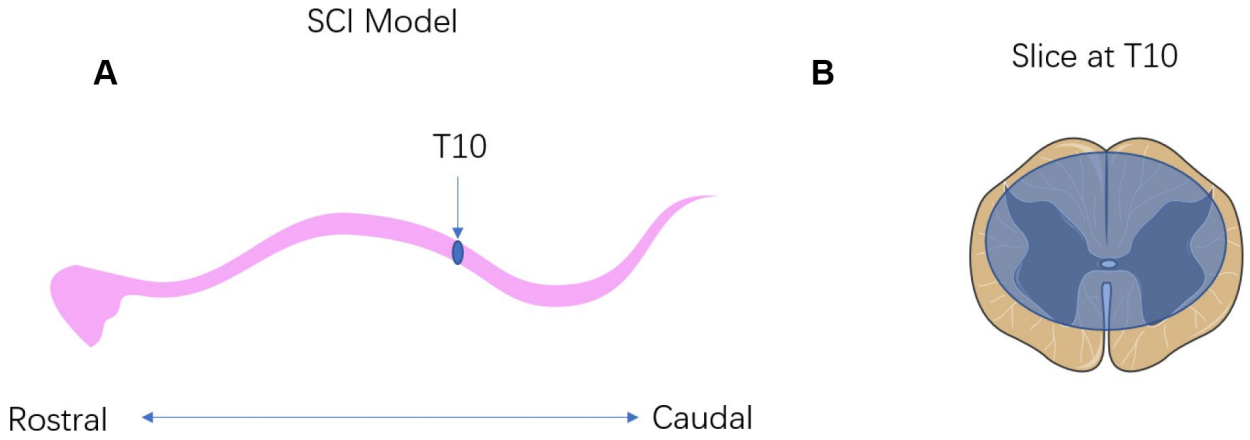

Supplementary Figure 2. Schematic of the SCI lesion area. (**A**) T10 (blue area) was crushed by modified Allen's weight drop apparatus; (**B**) The cross section of T10, blue area was injured.

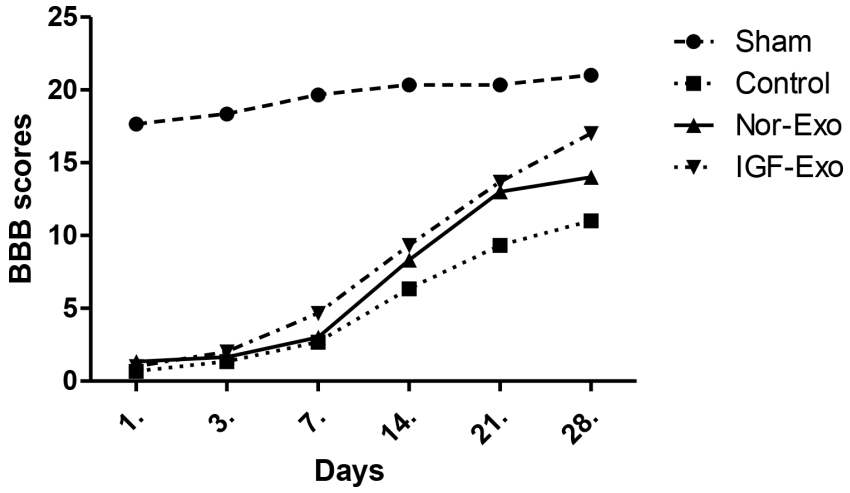

Supplementary Figure 3. BBB scores were used to assess locomotor behavior in rats 1, 3, 7, 14, and 28 days after SCI. The behavior function by BBB score at 1, 3, 7, 14 and 28 days after SCI.

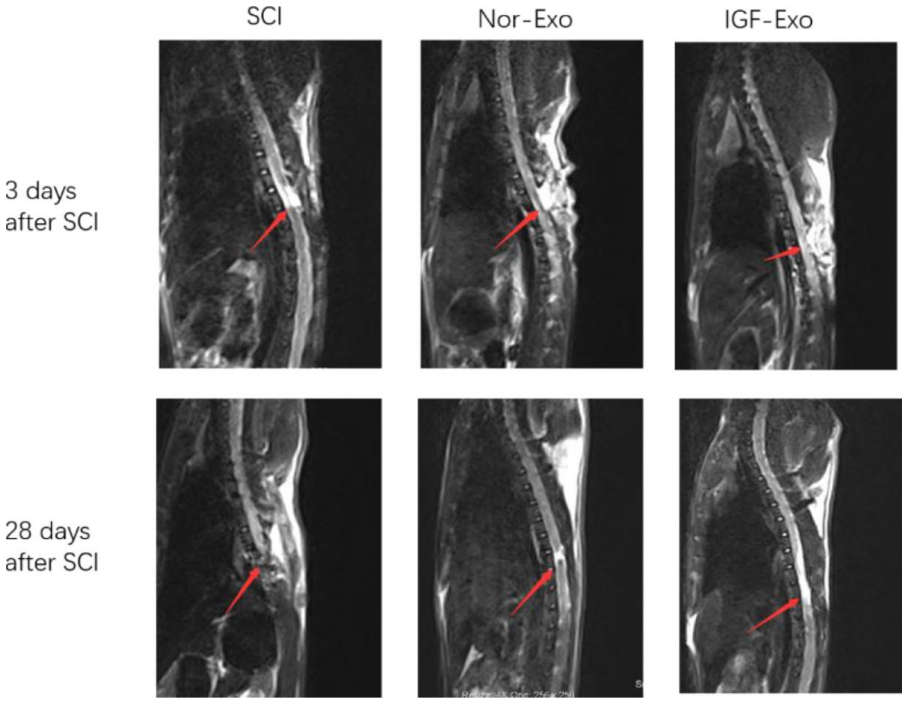

Supplementary Figure 4. The MRI image of SCI, Nor-Exo, and IGF-Exo groups. The T2 sequence of MRI at 3 days after SCI and 28 days after SCI. The red arrows point to the injury areas.

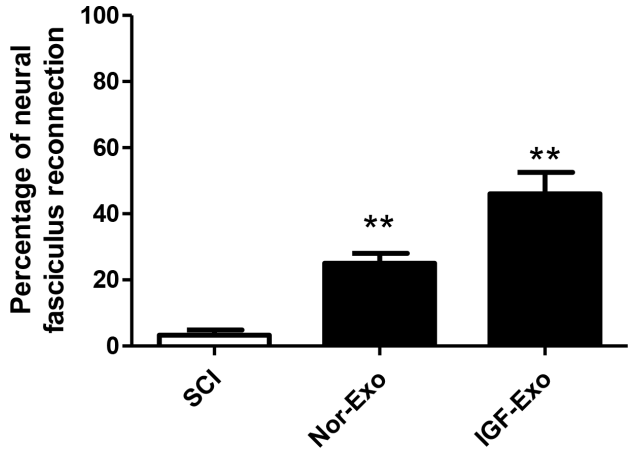

Supplementary Figure 5. Neural fasciculus reconnection percentages from DTI. The DTI sequence of MRI at 28 days after SCI showed the percentage of neural fasciculus reconnection of SCI, Nor-Exo, and IGF-Exo group. ***P*<0.01 for IGF-Exo vs. Nor-Exo.

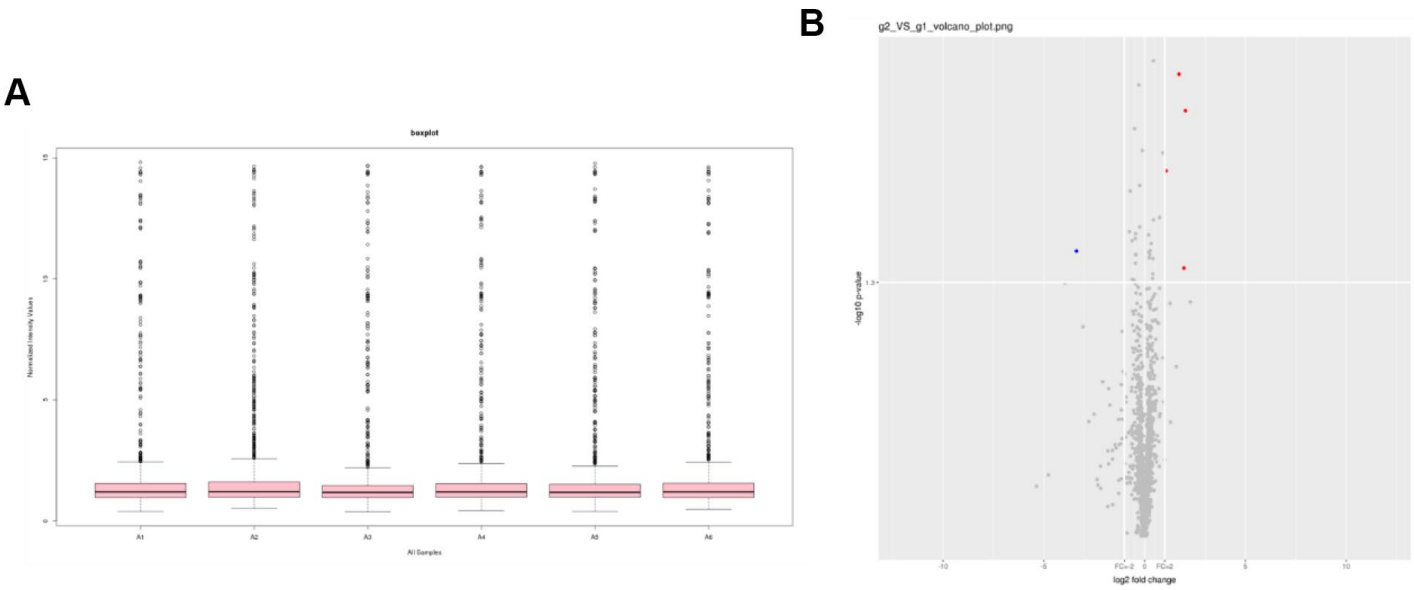

Supplementary Figure 6. miRNA sequence analysis of Nor-Exo and IGF-Exo. (**A**) all of the miRNA sequence results were subjected to normalized. (**B**) Volcano figure of miRNA sequence.